Vacuum 207 (2023) 111585

Contents lists available at ScienceDirect

Vacuum

journal homepage: www.elsevier.com/locate/vacuum

Selective atomic layer etching of Al_2O_3, AlN_x and HfO_2 in conventional ICP etching tool

V. Kuzmenko [a,*], Y. Lebedinskij [b], A. Miakonkikh [a], K. Rudenko [a]

[a] Valiev Institute of Physics and Technology of Russian Academy of Sciences, 34 Nakhimovsky av, 117218, Moscow, Russia
[b] Moscow Institute of Physics and Technology, 9 Institutskiy per, 141701, Dolgoprudny, Russia

ARTICLE INFO

Keywords:
Atomic layer etching
ICP plasma
Polymer deposition
Fluorocarbon radicals
Atomic fluorine

ABSTRACT

The atomic layer etching process of Al_2O_3, AlN_x and HfO_2 in conventional plasma etching tool was investigated. The etching process is based on surface modification by fluorocarbon film deposition from $Ar/CF_4/H_2$ plasma and subsequent activation of etching by Ar ion bombardment from plasma. The study of deposition process showed that varying plasma composition surface kinetics significantly change from deposition to etching. This is associated with the rise of fluorine concentration both in plasma and in deposited fluorocarbon film. Plasma mixture with low CF_4 fraction was chosen for modification step of ALE process because it provides low fluorinated film which does not etch SiO_2 and TiN improving selectivity to the potential mask material in etch process. The ALE process shows self-limiting characteristics providing the ALE process window at duration of modification step. The etch rate is 0.16 nm/cycle for Al_2O_3, 0.20 nm/cycle for AlN_x and 0.11 nm/cycle for HfO_2, which is close to monolayer mode. Relatively short cycle duration provides feasible etch rate in terms of time consumption. The significant selectivity over TiN (more than 20) was achieved allowing employing TiN as mask material for high resolution selective etching.

1. Introduction

Elements of integrated circuits are approaching atomic scales and new fabrication technologies providing atomic-scale accuracy in production are needed. This demands techniques of additive and subtractive formation of elements with an ultimate level of precision scalable to large wafer size up to 300 mm. Atomic layer deposition (ALD) of different materials based on successive stages repeated cyclically demonstrates perfect technological parameters: thickness control, high level of uniformity over the wafer, high level of step coverage, true monolayer mode of growth (no parasitic CVD reactions) [1]. Although the same idea of application cyclical successive multistep process for etching named atomic layer etching (ALE) was proposed decades ago [2], it is still lacks some advantages which, as expected, should be inherent in the atomic-layer nature of the process, such as perfect etch rate control, uniformity over the large wafer, close to unity level of synergy [3]. Although synergy and atomic scale etch rate control achieved in the neutral beam approach [4] were rather good, great efforts are being made to adjust ALE for application in wide aperture plasma source equipment [5]. Currently, variety of materials is studied for the possibility of ALE, and etching selectivity is also under the focus of research.

A number of studies devoted to ALE of different dielectrics were growing over the last years due to the requirements of manufacturers of integrated circuits and perspective electronic devices. Thin films of HfO_2 are typically used in the gate dielectric stacks of modern transistors. The application of the ALE process for etching HfO_2 improves transistor characteristics [6]. The drain current is 70% higher in an ALE-made transistor with a gate voltage of 1 V. Also, the off-state leakage current is almost an order of magnitude less. This is quite a significant improvement in transistor characteristics. ALE of aluminum oxide and nitride can find various applications in microelectronics. Thin films of Al_2O_3 or AlN_x are often used as interface passivation in high electron mobility transistors (HEMT) [4,7]. Precise etching of these films can be required for producing contacts to 2D electron gas. Another application for thin aluminum-containing films is the insulator in the Josephson junction, which can have various applications such as a very sensitive magnetometer and quantum computing [8,9]. The use of accurate etching technology should improve device characteristics, due to better structure controllability and fewer defects. Thus, realization of ALE of Al_2O_3, AlN_x, and HfO_2, in the microelectronic industry should enhance device performance.

The idea of the ALE process has much in common with the ALD

* Corresponding author.
E-mail address: kuzmenko@ftian.ru (V. Kuzmenko).

https://doi.org/10.1016/j.vacuum.2022.111585
Received 22 June 2022; Received in revised form 7 October 2022; Accepted 8 October 2022
Available online 17 October 2022

process. A cycle consisting of two main steps is repeated. The first step is a modification of the surface in which a saturated stable layer is formed. The second step is an activation of surface reaction between modified layer and material. The concept of the process is that both steps must be self-limiting. Ideally, there must be no effect of each step alone. Anisotropy of etching and at the same time self-limitation of activation process can be achieved by reaction activation by accelerated particles, which can stimulate a surface reaction but cannot sputter material. The range of process parameters, in which both steps are self-limited and etching occurs due to the interaction of steps, is called the ALE window. The etch rate does not change with variation of the process parameters in the ALE window range. Process in the ALE window produces low damage, resulting in better performance of structures. In fact, not complete saturation one of the steps leads to so called quasi-ALE process [5,10] in which the etch rate increases with the growth of step duration. In plasma etching tools, this occurs due to the non-monoenergetic distribution of ions. So, the smaller incline of the etch rate dependence, the process is closer to ideal ALE regime and process reproducibility is better.

One of possible mechanisms of surface modification which is widely employed on the first step of ALE is polymer film deposition from plasma [5,11]. The formation of polymer films is usually carried out by plasma of fluorocarbon gases (i.e. C_4F_8) or hydrofluorocarbons (i.e. CHF_3). The process based on the deposition from CHF_3 plasma and subsequent Ar bombardment showed satisfactory anisotropy of SiO_2 etching [5]. Also, according to Ref. [12], the ALE process with CH_4/C_4F_8 and CH_4/CHF_3 mixtures were compared and it was shown that CHF_3 based plasma allows achieving ALE process for HfO_2 films. The possibility of realizing of SiO_2 ALE process in ion beam source with polymer film deposition from C_4F_8 plasma was shown in Ref. [13]. An approach to SiO_2 ALE process in capacitively coupled plasma (CCP) reactor using Ar/CF_3I plasma for the surface modification and O_2 plasma for the reaction activation showed quite good saturation for deposition and removal steps duration [14], but the increase of surface roughness after etching was rather significant. The important result for understanding the mechanism of the self-limiting ALE process with polymer film deposition was shown in Ref. [15]. The study of SiO_2 ALE with C_4F_8/Ar plasma for modification and O_2 plasma for activation [15] demonstrated that despite not self-limiting deposition process in fluorocarbon plasma, the cyclic ALE process can be saturated. The authors explain that surface reaction between modified film and material is possible only in the limited thickness of the interface between fluorocarbon film and SiO_2 and excessive surface fluorination does not affect the ALE process. Therefore, fluorocarbon plasma is often used to etch silicon compounds due to the formation of silicon fluoride. However, the etch rate per cycle obtained in Refs. [5,15] are on the order of 1 nm. This shows that the interaction of the reactant with the etched surface occurs to a depth of several monolayers. Although this process is a quasi-ALE process, it will not give the benefits that are expected from a real ALE process. Moreover, cycle duration of the most proposed processes [10,14,15] is more than 2 min, which becomes a major barrier to commercial application, due to the fact that the ALE process could be the longest stage in the IC's production workflow.

In addition to silicon-containing compounds, it was shown that the thermal etching process by the formation of fluoride is feasible for Al_2O_3 [16] and AlN [17]. The etching process of Al_2O_3 with fluorine-containing plasma is also possible [18], but with relatively low etch rate. Thus, ALE etching of Al and Hf based compounds using surface fluorination can be realized.

Optimization and deep understanding of the physical and chemical processes in ALE require detailed study of the polymer film formation process. In Ref. [19] effect of DC bias for C_4F_8 and C_4F_6 plasma was studied for the SiO_2 etching process. Without DC bias polymer film is deposited on SiO_2, with the increase of DC bias deposition process goes into etching mode through an equilibrium film. The same effect was observed in Ref. [20] for etching Si, SiO_2, Si_3N_4, and SiCH in C_4F_8 and CHF_3 plasma. These results illustrate that by changing plasma parameters it is possible to change equilibrium from deposition to etching on different materials.

Another mechanism for changing the balance between deposition and etching in fluorocarbon plasma is the addition of H_2 into the plasma mixture. The effect of the addition of H_2 into CF_4 plasma on the etching of Si and SiO_2 was investigated [21]. In CF_4 plasma without DC bias Si and SiO_2 are etched with a relatively high etching rate, but with the increase of H_2 in plasma mixture etching is stopped and polymer deposition occurs. So, CF_4/H_2 plasma mixture should provide the possibility of fine-tuning the surface kinetics. The role of hydrogen on polymer film deposition in fluorocarbon ICP was studied previously [22]. Results showed that even at high fraction of CH_2F_2 in plasma mixture concentration of methane family particles are much lower than fluorocarbon family particles. This is due to the multistep formation kinetics for CH_x species and the lack of hydrogen atoms which are effectively consumed in reactions: $CF_3+H\rightarrow HF + CF_2$ and $CF_2+H\rightarrow HF + CF$. The major hydrogen-containing particle is HF which formation consumes F radical, and, consequently decreases fluorine concentration significantly. So, the role of hydrogen is to change balance between polymer-forming and etching-responsible particles in plasma, which leads to the change of equilibrium between etching and deposition on the surface.

The record of introducing new technologies into commercial microelectronics shows that their application begins only when it is possible to scale the technology on a full-wafer scale. The scaling of integrated circuit manufacturing processes allows reducing production costs and, consequently, the price of products. Approach to ALE which uses beam sources has a drawback for industry integration due to difficulties with scaling. Plasma etching process should be more preferable and uniformity across the wafer is important parameter of etching process. The number of total etch steps increases with the decrease of technology node and the tolerance for variation is traditionally about 10% and shrinks with each technology node [23].

Efforts are being made to optimize plasma tools for the ALE process in terms of optimizing the fast gas supply and pumping system (similar to other tools for multi-stage plasma processes) and optimizing the energy distribution of ions bombarding the surface to reduce its width. When the RF bias applied to the sample, ion energy distribution function has bimodal shape, which width increases with the growth of ion energy and can reach 40 eV, while applying low frequency specially tailored voltage impulses makes it possible to narrow the energy distribution at high energies, although, at low ion energy (about 20 eV), distribution width remains the same (~7 eV) for sinusoidal and tailored bias [24].

This work is devoted to the study of the approach to ALE in which the surface is modified by polymer fluorocarbon film deposition in a conventional inductively coupled plasma (ICP) tool. The studied materials for ALE were Al_2O_3, AlN_x, and HfO_2. The selectivity was studied relative to TiN and SiO_2, as these materials can be used either as hard masks, or the etching stop-layer for target materials in some applications. Moreover, according to Ref. [25] SiO_2 is similar in terms of etching to the widespread material of e-beam resist mask hydrogen-silsesquioxane (HSQ). Initially, polymer film deposition from plasma was studied in order to select a mode that would allow one to achieve selectivity. The thickness of deposited fluorocarbon film was measured on each material by spectral ellipsometry, and composition of the polymer films was evaluated using X-ray photoelectron spectroscopy (XPS). The process of film deposition and their analysis was also carried out on the surface of Si. Diagnostics of fluorocarbon plasma were conducted to explain the deposition and the etching processes occurring on the surface. The radical concentration was estimated using optical emission actinometry with a help of data received from the Langmuir probe diagnostics. The ALE process was investigated for chosen fluorocarbon film deposition regime.

2. Experimental

2.1. Polymer deposition and plasma etching experiments

The atomic layer etching process was realized in the conventional plasma etching tool Plasmalab 100 (OIPT, UK). The cylindrical aluminium process chamber is 450 mm high and 380 mm in diameter. The plasma is excited by the coil around the chamber. The coil is powered by an RF generator (2 MHz) using a matching box. Walls are made from aluminium and ICP power is injected to the discharge through the dielectric window. Wafer is fixed on the table using wafer chuck. RF generator (13.56 MHz) with matching box provides DC bias on the wafer. The chamber is pumped out by a turbomolecular pump to a base pressure 10^{-6} Torr. Process gases are introduced to the chamber with mass flow controllers. Aluminum oxide, hafnium oxide and aluminum nitride films were deposited on the silicon (100) wafers (p-type, 10 Ohm·cm) by ALD (FlexAl, OIPT, UK). Wafers were cut into 2 × 2 cm coupons (except the case when the full 100 mm wafer was etched). The coupons were glued by PFPE grease to a 100 mm silicon wafer used as a sample carrier. The He pressure up to 6–7 Torr were built during the etching under the carrier to provide good thermal contact with the table. Film thickness was measured on each sample before and after the plasma process with spectral ellipsometry on M-2000X tool (J.A. Woollam Co., Inc., USA) with range 250–1000 nm, using Cauchy model.

F/C ratio of deposited polymer films was estimated by X-ray photoelectron spectroscopy (XPS). For XPS studies, separate samples of films were deposited in different plasma conditions in continuous plasma for 4–7 min on silicon (100) 2 × 2 cm coupons (p-type, 10 Ohm·cm). Film thickness was 11–22 nm. This thickness was chosen for reliable signal detection from the components of the bulk film. XPS measurements were made on Theta Probe spectrometer (Thermo Fisher Scientific, USA) with Al Kα (1486.6 eV) x-ray source. The base pressure during spectra acquisition was $2{\cdot}10^{-9}$ Torr. The total acquisition time of the spectra was 1.5–3.5 min. The binding energy scale was calibrated using the Au $4f_{7/2}$ (84 eV) line. The size of analyzed area was 0.4 mm, the electron emission angle was 50° relative to the normal. During the measurements, a standard charge neutralizer of the Theta Probe spectrometer - Flood Gun was used, which produces a flow of electrons and Ar^+ ions with an energy of 2 eV. C(1s) and F(1s) lines were measured and approximated with a set of Gaussian peaks. The F/C ratio was estimated by two approaches: 1) by ratio F(1s)/C(1s) and 2) by proportion of carbon states obtained by the deconvolution of C(1s) band. The role of adventitious carbon is important in determining the F/C ratio in polymer films [26]. In our work samples were produced in the same technological route in sequence, were stored in the same container for the same time, and were analyzed simultaneously, so we hope that role of adventitious carbon should be approximately similar, and qualitative difference in determined F/C ratio is due to the difference in deposition regimes. Another problem of XPS measurements is the need to perform charge referencing [26], which leads to a shift in the energy scale due to the charge on the surface of the sample. In our case, the thickness of the polymer film (11–22 nm) did not allow observing silicon lines from the substrate, therefore, it was not possible to perform internal referencing using Si peaks. Measured XPS spectra have pronounced peaks in the interval of 689.8–690.2 eV, which was identified by other authors as F (1s) peaks using binding energy calibration and referencing by Au spectra [27]. In our work, F(1s) peak was used for internal referencing. At C(1s) spectra peaks with energy at 285.5 eV, 288.0 eV, 290.2 eV, 292.4 eV, and 294.6 eV were detected. In the same work [27] C(1s) peak was observed at 290.1 eV at CF-like compound. The peaks with binding energies 290.6 eV, 292.0–292.8 eV and 294.6–294.8 eV were ascribed to CF, CF_2 and CF_3, respectively [28,29], where F(1s) peak was used for internal referencing as it shows only one distinct peak and values of binding energy of F(1s) in CF_2-type compounds in the literature are quite comparable.

After the investigation of the deposition process, the cyclic etching process with optimized deposition parameters was studied (Fig. 1). The typical cycle consisted of 0–15 s deposition process (modification step) which was performed in $Ar/CF_4/H_2$ ICP with no DC bias on the wafer. Then the reactor was purged with argon for 10 s. After that, DC bias was applied in Ar ICP plasma for 0–20 s. Argon flow was constant during the whole process and was 50 sccm and CF_4 and H_2 flows were varied 2–20 sccm. ICP power was 1500 W throughout the process. The table temperature was kept constant at 20 °C.

2.2. Langmuir probe diagnostics

Langmuir probe diagnostics is a useful method for determination of plasma charged-particles related properties, which is important for kinetics understanding and radical concentration calculation. Measurements of I–V curves were made with ESPion Advanced probe (Hiden Analytical, UK) in −100 - +20 V range with 0.1 V step. The cylindrical tungsten probe was 10 mm in length and 0.3 mm in diameter. The measuring probe is mounted on a long (~200 mm) dielectric holder, which makes it possible to carry out measurements in the central region of the discharge. In order to prevent polymer contamination on the probe surface, between the measurements, the probe was maintained at a potential of −15 V and was cleaned with an ion current bombardment, which allows obtaining undisturbed probe characteristics [30]. Probe size measurements before and after plasma diagnostics prove invariability of feature size (no probe material etching takes place during measurements). The electron temperature, plasma potential and electron and positive ion concentration were calculated from the I–V characteristics. The ion current was determined using orbital-motion-limited (OML) theory [31]. The ion current branch of I–V characteristic was approximated by the expression $I \sim V^{\alpha}$. The deviation of α from 1/2, predicted by OML theory, was less than 20%, which indicates the validity of applying OML theory. Subtracting the ion current from I–V characteristics gives the electron current. The second derivative of electron current over potential is proportional to the electron energy distribution function and linear dependence of the natural logarithms of electron current with the probe potential corresponds to Maxwellian electron energy distribution. The electron temperature was calculated by the slope of the natural logarithm of electron current versus probe potential.

2.3. Optical emission spectroscopy

By means of plasma optical emission spectroscopy neutral particles, which of greatest interest for understanding the kinetics of deposition and etching, can be identified, such as F [32], CF [33], and CF_2 [34]. According to Ref. [35] CF and CF_2 are predominant particles responsible for fluorocarbon film formation and F radical is responsible for the etching process.

Concentration of neutral radicals was evaluated using the spectrometric method of optical emission actinometry. Emission spectra were measured with Ocean Insight HR4Pro in wavelength range 200–900 nm with optical resolution 0.7 nm. Intensities of F and CF_x radicals, which are relevant for understanding mechanism of polymer film deposition, were determined. Overlapping of CF_2 (A^1B_1-X^1A_1) bands and CF_2^+ continuum [36] can be observed in 235–270 nm wavelength range. In our work CF_2^+ continuum baseline was extracted from the spectra in order to calculate intensity of CF_2 (A^1B_1-X^1A_1) bands. Ar 750.4 nm line was used as actinometer line for measurement of F, CF_x concentration before [32–34]. Application of Ar 750.4 nm line for actinometry of CF and CF_2 was proved in Ref. [33] by independent laser induced fluorescence (LIF) measurements. The concentration of CF_2 radicals was calculated by the intensity of A^1B_1-X^1A_1 band [34] and CF by $B^2\Delta$-$X^2\Pi$ band. According to Ref. [32], excitation of higher state of F 685.6 nm and Ar 750.4 nm lines is produced by direct electron impact in similar conditions. Due to low pressure (10 mTorr), time between collisions in our case is much higher than radiative time of mentioned transitions, that is why collisional

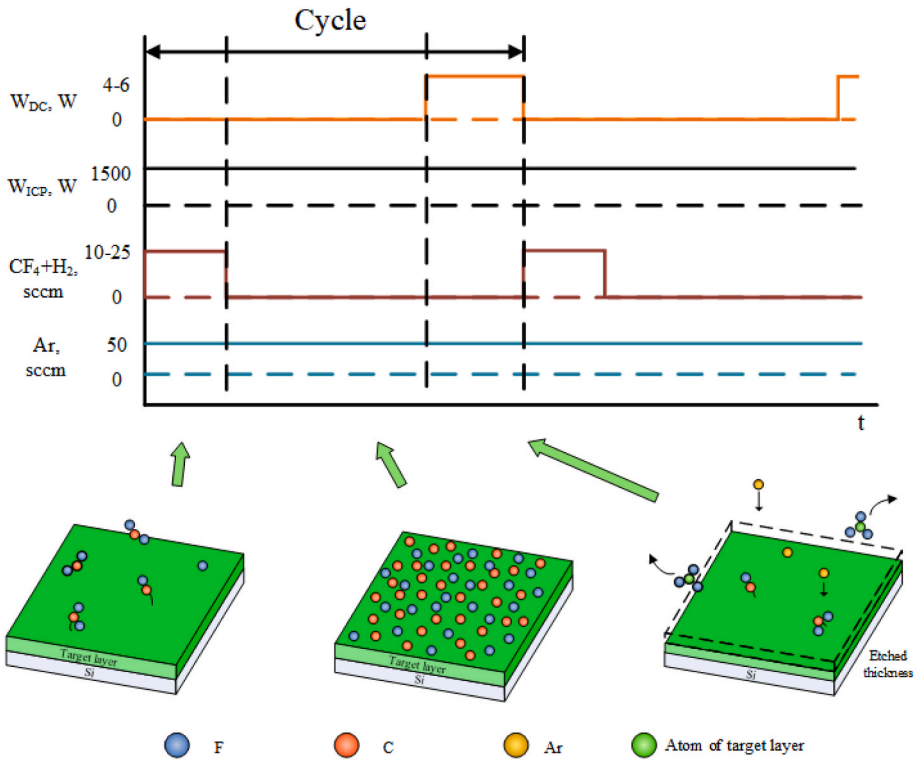

Fig. 1. Parameter sequence in ALE process (on the schematic diagrams are shown the states of the etched surface are shown: 1) building the polymer film on the surface (modification step), 2) saturated continuous film on the surface, 3) surface reaction between the polymer and the target layer activated by argon (activation step)).

quenching of the excited states can be omitted. So, concentration of neutral radicals can be estimated as [34]:

$$[X] = [Ar]\frac{k_{Ar} \bullet \lambda_X \bullet \int I_X(\lambda)d\lambda}{k_X \bullet \lambda_{Ar} \int I_{Ar}(\lambda)d\lambda}$$

Where [X], [Ar] – concentration of X and Ar radicals, k_X, k_{Ar} - direct electron impact excitation rates, λ_X, λ_{Ar} – wavelengths of corresponding transitions. Electron impact excitation rates were calculated using electron temperature measured by Langmuir probe and cross sections taken from Refs. [32,37].

3. Results and discussion

3.1. Polymer film deposition investigation

Fluorocarbon film deposition process in $Ar/CF_4/H_2$ plasma was studied at different quantitative composition of the plasma mixture. Chamber pressure was 10 mTorr. Plasma was generated by 1500 W ICP power without applying DC bias on the table. In the first series of measurements, the Ar fraction was kept constant at 83.3% and fraction of CF_4 (ν_{CF4}) were varied (3.3%–13.3%) and the rest was H_2. The deposition rate on different materials measured by *ex situ* spectral ellipsometry over CF_4 fraction in plasma mixture is shown in Fig. 2 a. At low ν_{CF4} (<5%) we observe that fluorocarbon film deposits on all studied materials. With the increase of CF_4 fraction, the deposition rate growth first and then reaches a maximum. Further increase of ν_{CF4} leads to decrease of deposition rate on Si, Al_2O_3, HfO_2, and AlN_x and even change balance from deposition to etching on SiO_2 and TiN.

In order to explain deposition rate behavior plasma diagnostics was made. Langmuir probe diagnostics were carried out in each plasma conditions and the natural logarithms of electron current were linear with the probe potential, which allows us to consider the Maxwellian electron energy distribution function. The electron temperatures insignificantly change depending on the plasma composition in the selected ranges. The values of electron temperatures were 3.1–3.3 eV. Knowing

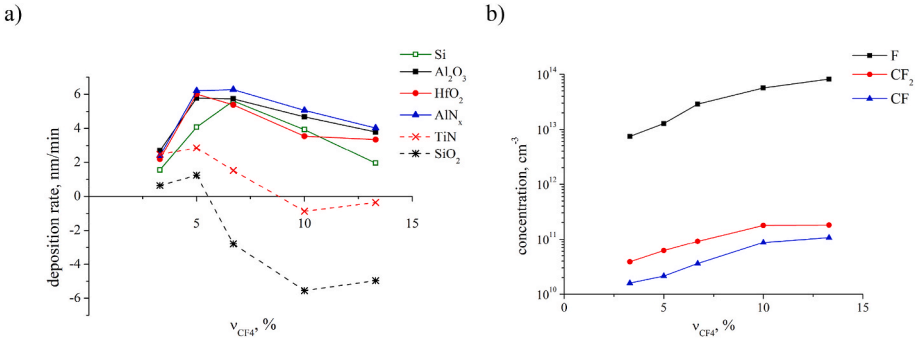

Fig. 2. a) Film deposition rate on different materials and b) radicals concentration over ν_{CF4} in the plasma mixture, while Ar fraction is 83.3%. Negative values correspond to etching.

the values of electron temperatures, the excitation rates and, consequently, the concentrations of radicals F, CF and CF_2 were calculated (Fig. 2 b). Fluorine-containing radicals concentration increase with the growth of CF_4 fraction in plasma mixture. Polymer-forming molecular radicals concentration grows less than F radical concentration. At low CF_4 fractions the increase of CF and CF_2 radical concentrations consists with the growth of polymer film deposition rate. With the increase of CF_4 fraction significant rise of fluorine radical concentration relatively to CF_x concentration change surface kinetics balance towards etching.

The increase of fluorine with the rise of CF_4 fraction was also observed in the composition of polymer films deposited on silicon by XPS. F(1s) and C(1s) peaks of polymer films deposited in different conditions are shown in Fig. 3. Fig. 3 a shows the observed position of the fluorine line F(1s), which we used as internal reference. Although it is influenced by chemical bonding, analysis of the literature shows that energy of F(1s) peak for fluorocarbon films $(-CF_2-CF_2-)_n$ is quite narrow interval of 689.4–690.3 eV [38]. In the present study the observed position of F(1s) 689.8–690.2 eV which shows that there is no significant shift in the XPS spectra due to the sample charging.

On Fig. 3 b different Gaussian peaks corresponding to chemical carbon bonds can be observed on films deposited in Ar(83.3%)/CF_4(3.3%)/H_2(13.4%) and Ar(83.3%)/CF_4(6.6%)/H_2(10.1%) plasma. The peak at 285.5 eV was ascribed to C-CF_n bond [39], 290.2 eV, 292.4 eV, and 294.6 eV peaks were attributed to CF, CF_2 and CF_3, respectively [27–29]. The film deposited in higher CF_4 fraction plasma has more pronounced C-F_x peaks corresponding to higher concentration of C-bonded fluorine in film. The F/C ratio determined by C (1s) deconvolution increases from about 0.5 to 1.6 as the CF_4 fraction rises from 3.3% to 6.6%. C(1s) peak at 288.0 eV observed on film deposited in Ar (83.3%)/CF_4(6.6%)/H_2(10.1%) plasma can possibly be associated with either some hydrocarbon group, or another condition of CF bond [28], so F concentration can be a bit underestimated. However, this peak is observed only on film deposited in higher CF_4 fraction plasma, so the qualitative result of increasing the concentration of fluorine in the films with the rise of CF_4 fraction in plasma from 3.3% to 6.6% is still valid. Intensity of F(1s) peak increased twice with the growth of CF_4 in plasma (Fig. 3 a). The F (1s)/C (1s) ratio also rises from 2 to about 4. Increase of fluorine concentration in polymer film agrees with the behavior of radical concentration in plasma and confirms change of surface kinetics towards etching. That is why low CF_4 deposition regime is preferable for surface modification step for ALE process.

In the second series, the Ar fraction was varied at constant CF_4/H_2 ratio, in order to increase deposition rate for modification step of ALE process. Low CF_4/H_2 ratio regime with $CF_4/H_2 = 0.25$ was chosen due to the character of surface deposition kinetics. Spectral ellipsometry showed that deposition rate monotonously increases with the decrease of Ar fraction from 83.3% to 66.6% on all materials. This can be attributed with the decrease of F radical concentration and the growth of polymer-forming particles concentration relatively to fluorine radicals which was observed by optical emission actinometry.

During the surface modification step of the ALE process no etching of target material, mask, or sublayer should occur in order to ensure an acceptable selectivity of etching process. Also, polymer film deposition rate should be high enough to achieve fast ALE process. Hence, low CF_4/H_2 ratio and relatively low Ar fraction plasma (Ar(66.6%)/CF_4(6.7%)/H_2(26.7%)) mixture was chosen further for ALE modification step.

3.2. ALE process investigation

In this work, surface modification step was performed in Ar(66.6%)/CF_4(6.7%)/H_2(26.7%) plasma. The etch rate for different duration of modification and activation steps, was measured after 40 cycles ALE processes. The activation of surface reaction should not lead to sputtering of the material. According to Ref. [18] sputtering threshold for Al_2O_3 in fluorine containing plasma is about 20 eV and 50 eV for Ar plasma. Sputtering threshold for HfO_2 is much higher about 100 eV for Ar and 80 eV for fluorine containing plasma [40].

We performed preliminary research of etch rate depending on bias on the activation step for 12, 16 and 19 V and plasma potential equal to 18 V (measured by Langmuir probe). At 12 V bias no etching of HfO_2 was observed and the etch rate of Al_2O_3 was negligible slow (~0.04 nm/cycle). This is probably due to too small energy for surface reaction activation. Appling 19 V DC bias the etch rate grows much faster compared to 16 V. This is attributed to the increase in sputtering at this energy. So, in the further experiments the activation step was conducted in Ar plasma applying 16 V DC bias to the wafer and the etch rate of Al_2O_3 was ~0.16 nm/cycle.

Variation of modification step duration was at constant duration of activation step 10 s. At low duration of modification step (Fig. 4 a), surface is not modified completely and the etch rate is low. Insignificant etch rate at zero modification step confirms minimal effect of sputtering by argon ions. The etch rate of TiN does not depend on modification step duration remain close to zero nm/cycle value. As deposition rate of fluorocarbon on TiN was close to the value for the other materials, no etching was observed, possibly due to the lack of surface reaction activation. SiO_2 etch rate does not show evident ALE window with only slight plateau between 10 and 12 s duration. Very low etch rate of TiN and high etch rate of SiO_2 is probably connected with the differences between phase change points of titanium fluoride ($T_{sublimation} \sim +284$ °C [41]) and silicon fluoride ($T_{boiling} = -86$ °C [42]). In studied process desorption of surface reaction products stimulated by Ar ions with about 16 eV energy. As titanium fluoride is much less volatile, desorption of reaction products is difficult and etch rate is much slower. Another possible reason is significant role of the sputtering of SiO_2 by Ar ions compared with TiN and the other materials. SiO_2 sputtering rate, determined as a etch rate in the process with zero modification step

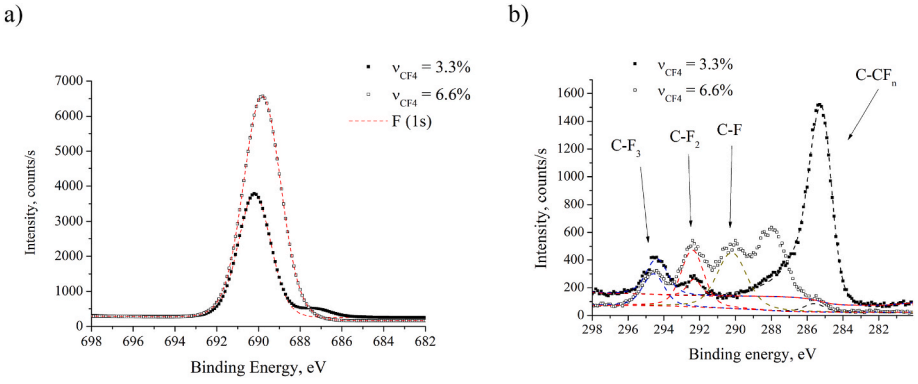

Fig. 3. XPS a) F(1s) and b) C(1s) profiles for 1) for film (11 nm) deposited in $\nu_{CF4} = 3.3\%$ (solid symbols) and 2) for film (22 nm) deposited in $\nu_{CF4} = 6.6\%$ (open symbols), while Ar fraction is 83.3%.

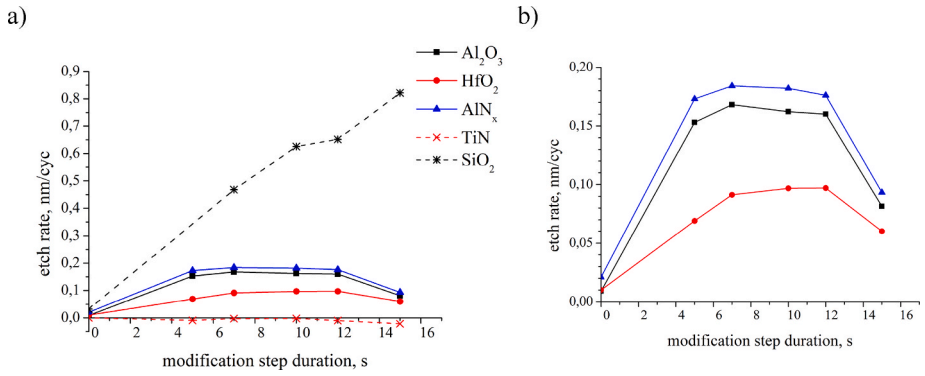

Fig. 4. The etch rate over modification step duration a) for all studied materials, and b) enlarged for Al_2O_3, AlN_x, and HfO_2.

duration, is about two-three times higher than sputtering rate of the other studied materials.

With the increase of modification step duration, the etch rate of Al_2O_3, AlN_x and HfO_2 reaches saturation, providing the ALE window (Fig. 4 b). Further rise of modification step leads to the decrease of the etch rate due to too thick film deposition. Thick film is sputtered at the start of ion bombardment step which decrease duration of the surface activation process and leads to incomplete surface reaction. Evident ALE window is observed in selected conditions between 5 and 12 s duration of surface modification step.

At constant modification step duration 10 s, results of variation of activation step duration is shown in Fig. 5. Without any activation step polymer film with thickness about 0.5 nm deposits at each cycle. At the start of activation step polymer film is etched. When activation step duration is enough to sputter top layer of modified film, following bombardment by argon ions leads to etching of material. The ALE window here is not so pronounced, probably due to non-monoenergetic ion distribution function. The incline of the etch rate dependence for HfO_2 2 times low than for Al_2O_3 corresponding to the higher sputtering threshold. The slight incline of dependences could provide moderate process unrepeatability from cycle to cycle.

The effect of purge step duration between modification and activation steps was examined. The process with doubled purge step duration 20 s was conducted. The change of etch rate compared with standard process with 10 s purge step was less than 10%. This indicates that 10 s purge is enough in our conditions to suppress all processes associated with steps mixing and following increase of purge step duration is unnecessary.

Having defined major cycle parameters, process with optimal parameters was studied. Duration of both modification and activation steps were 10 s. The etch depth dependence linearly increases with the number of cycles in the process (Fig. 6) and intercept of dependences was not detected. The values of etch rates, determined as a slope of the etch depth over number of cycle dependences, are 0.16 nm/cycle, 0.20 nm/cycle and 0.11 nm/cycle for Al_2O_3, AlN_x, and HfO_2 respectively. The SiO_2 etch depth has significant dispersion due to absence of clear ALE window and, consequently, poor repeatability from cycle to cycle. The average etch rate of SiO_2 and TiN are about 0.62 nm/cycle and 0.006 nm/cycle, respectively.

The etch rate per cycle achieved in ALE process are comparable with Al–O bond length equals 0.169 nm [43], which indicates close to single atomic precision regime. The etch rate in the term of time is quite acceptable for atomic scale processing (~0.3 nm/min and ~0.4 nm/min for Al_2O_3 and AlN_x, respectively) due to relatively low cycle duration after optimization. The linearity of etching process provides the ability to control etching process with sub nanometer scale accuracy. The selectivity of etching of Al_2O_3, AlN_x and HfO_2 over TiN is about 30, 40 and 20, respectively.

To the uniformity of ALE across the wafer the process was conducted on 100 mm wafer covered with Al_2O_3. The film thickness was measured in central 65 mm part of the wafer before and after etching using automatic system of spectral ellipsometry measurements. The etch rate decreases to the edge (Fig. 7) of the wafer and uniformity is about±3% minimum to maximum. A bit discrepancy of the etch rate value calculated from the linearity of etch depth measured on 2 × 2 cm samples and on whole wafer can be explained by the loading effect. In our case, this discrepancy is less than 20% and should be even less if open surface of

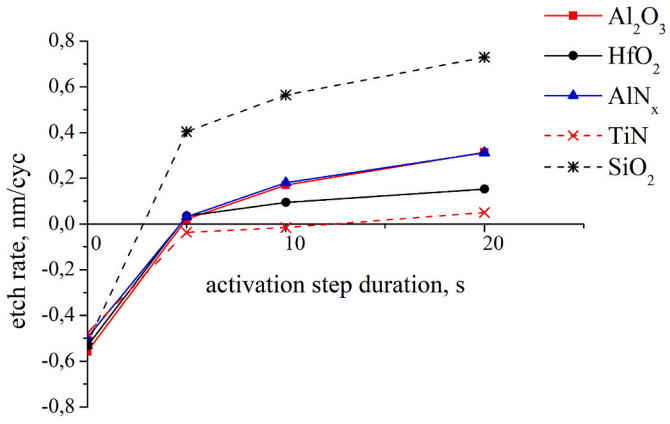

Fig. 5. The etch rate over activation step duration. Negative values correspond to film formation.

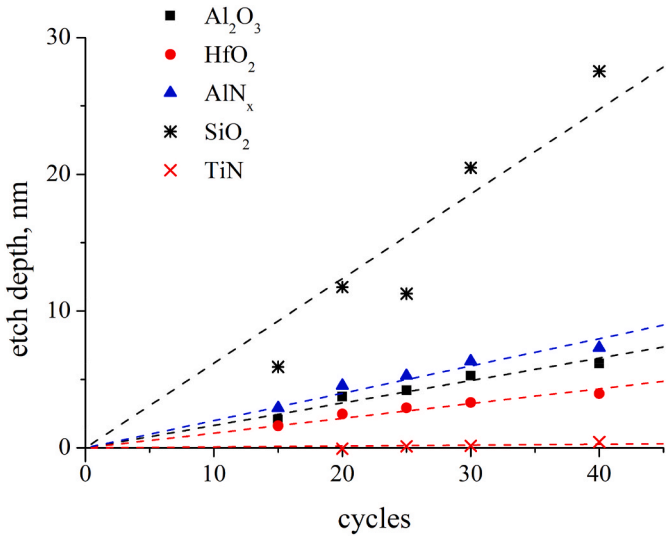

Fig. 6. The etch depth over the number of cycles in ALE process (activation step duration is 10 s).

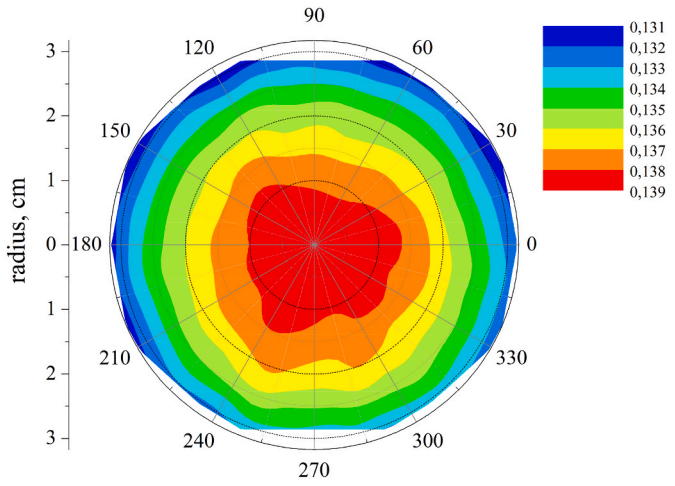

Fig. 7. The Al_2O_3 etch (nm/cycle) rate distribution across the wafer. The ordinate axis is the radius from the center of the wafer. The numbers around are the polar angle.

Al_2O_3 does not change significantly. Since the rate of formation of a fluorocarbon film depends on the area of the etched material, it may be necessary to adjust the duration of the stages during the ALE process compared to etching samples without a mask.

4. Conclusion

In this work the ALE process of Al_2O_3, AlN_x and HfO_2 in conventional plasma etching tool was investigated. The etching process is based on surface modification by fluorocarbon film deposition from $Ar/CF_4/H_2$ plasma and subsequent activation of etching by Ar ion bombardment from plasma. The study of deposition process showed that varying plasma composition surface kinetics significantly change from deposition to etching. This is associated with the rise of fluorine concentration both in plasma and in deposited fluorocarbon film. Plasma mixture with low CF_4 fraction was chosen for modification step of ALE process because it provides low fluorinated film which does not etch SiO_2 and TiN improving selectivity to the potential mask material in etch process. The ALE process shows self-limiting characteristics providing the ALE process window at duration of modification step. Activation by applying DC bias in argon plasma allows reduce the degree of dependence of the etching rate on the duration of the activation step. The small value of this slope is consistent with good cycle reproducibility. The etch rate is 0.16 nm/cycle for Al_2O_3, 0.20 nm/cycle for AlN_x and 0.11 nm/cycle for HfO_2, which is close enough to interatomic distance in these materials. Relatively short cycle duration provides feasible etch rate in terms of time. The significant selectivity over TiN (more than 20) was achieved allowing to employ TiN as mask material for high resolution selective etching. The good linearity of etched depth dependence on the number of cycles process implies good reproducibility (from cycle to cycle) and makes it possible to control etch depth with sub nanometer accuracy. The ALE process is adopted to commercial tool compatible with the industry. Without any tool modification moderate uniformity across the wafer consistent with typical values was achieved.

CRediT authorship contribution statement

V. Kuzmenko: Writing – original draft, Investigation, Formal analysis, Data curation. **Y. Lebedinskij:** Formal analysis. **A. Miakonkikh:** Writing – review & editing, Project administration, Methodology, Funding acquisition. **K. Rudenko:** Writing – review & editing, Supervision, Project administration.

Declaration of competing interest

The authors declare that they have no known competing financial interests or personal relationships that could have appeared to influence the work reported in this paper.

Data availability

Data will be made available on request.

Acknowledgments

The investigation was supported by the Program no. FFNN-2022-0020 (in part of high-k dielectrics etching), FFNN-2022-0019 (in part of technological process development) of the Ministry of Science and Higher Education of Russia for Valiev Institute of Physics and Technology of RAS and partially supported Russian Foundation for Basic Research grant No. 20-07-00832A (in part of plasma diagnostics).

References

[1] B. Kim, N. Lee, J. Lee, T. Park, H. Park, Y. Kim, C. Jin, D. Lee, H. Kim, H. Jeon, Remote plasma enhanced atomic layer deposition of titanium nitride film using metal organic precursor (C12H23N3Ti) and N2 plasma, Appl. Surf. Sci. 541 (2021) 148482, https://doi.org/10.1016/j.apsusc.2020.148482.

[2] K. Suzue, T. Matsuura, J. Murota, Y. Sawada, T. Ohmi, Substrate orientation dependence of self-limited atomic-layer etching of Si with chlorine adsorption and low-energy Ar+ irradiation, Appl. Surf. Sci. 82/83 (1994) 422, https://doi.org/10.1016/0169-4332(94)90252-6.

[3] K.J. Kanarik, S. Tan, W. Yang, T. Kim, T. Lill, A. Kabansky, et al., Predicting synergy in atomic layer etching, J. Vac. Sci. Technol. 35 (2017), 05C302, https://doi.org/10.1116/1.4979019.

[4] K. Min, S. Kang, J. Kim, Y. Jhon, M. Jhon, G. Yeom, Atomic layer etching of Al2O3 using BCl3/Ar for the interface passivation layer of III–V MOS devices, Microelectron. Eng. 110 (2013) 457–460, https://doi.org/10.1016/j.mee.2013.03.170.

[5] S. Dallorto, A. Goodyear, M. Cooke, J. Szornel, C. Ward, C. Kastl, A. Schwartzberg, I. Rangelow, S. Cabrini, Atomic layer etching of SiO2 with Ar and CHF3 plasmas: a self-limiting process for aspect ratio independent etching, Plasma Process. Polym. 16 (9) (2019), 1900051, https://doi.org/10.1002/ppap.201900051.

[6] J. Park, W. Lim, B. Park, I. Park, Y. Kim, G. Yeom, Atomic layer etching of ultra-thin HfO2 film for gate oxide in MOSFET devices, J. Phys. Appl. Phys. 42 (5) (2009), 055202, https://doi.org/10.1088/0022-3727/42/5/055202.

[7] S. Zhao, X. Liu, L. Zhang, H. Huang, J. Shi, P. Wang, Impacts of thermal atomic layer-deposited AlN passivation layer on GaN-on-Si high electron mobility transistors, Nanoscale Res. Lett. 11 (1) (2016), https://doi.org/10.1186/s11671-016-1335-7.

[8] J. Meckbach, M. Merker, S. Buehler, K. Ilin, B. Neumeier, U. Kienzle, et al., Sub-μm Josephson junctions for superconducting quantum devices, IEEE Trans. Appl. Supercond. 23 (3) (2013), https://doi.org/10.1109/tasc.2012.2231719, 1100504-1100504.

[9] K. Makise, R. Sun, H. Terai, Z. Wang, Fabrication and characterization of epitaxial TiN-based Josephson junctions for superconducting circuit applications, IEEE Trans. Appl. Supercond. 25 (3) (2015) 1–4, https://doi.org/10.1109/tasc.2014.2364214.

[10] K. Koh, Y. Kim, C. Kim, H. Chae, Quasi atomic layer etching of SiO2 using plasma fluorination for surface cleaning, J. Vac. Sci. Technol.: Vacu, Surf. Films. 36 (1) (2018), 01B106, https://doi.org/10.1116/1.5003417.

[11] V. Kuzmenko, A. Miakonkikh, K. Rudenko, Cyclic discrete etching of Silicon oxide in deposition-sputtering cycles: towards to ALE, Proc. SPIE 11022 (2019), 1102225, https://doi.org/10.1117/12.2522472.

[12] K. Lin, C. Li, S. Engelmann, R. Bruce, E. Joseph, D. Metzler, G. Oehrlein, Selective atomic layer etching of HfO2 over silicon by precursor and substrate-dependent selective deposition, J. Vac. Sci. Technol. 38 (3) (2020), 032601, https://doi.org/10.1116/1.5143247.

[13] S. Kaler, Q. Lou, V. Donnelly, D. Economou, Atomic layer etching of silicon dioxide using alternating C4F8 and energetic Ar+plasma beams, J. Phys. Appl. Phys. 50 (23) (2017), 234001, https://doi.org/10.1088/1361-6463/aa6f40.

[14] S.Y. Kim, In-Sung Park, J. Ahn, Atomic layer etching of SiO2 using trifluoroiodomethane, Appl. Surf. Sci. 589 (2022) 153045, https://doi.org/10.1016/j.apsusc.2022.153045.

[15] T. Tsutsumi, H. Kondo, M. Hori, M. Zaitsu, A. Kobayashi, T. Nozawa, N. Kobayashi, Atomic layer etching of SiO2 by alternating an O2 plasma with fluorocarbon film deposition, J. Vac. Sci. Technol.: Vacu, Surf. Films. 35 (1) (2017), 01A103, https://doi.org/10.1116/1.4971171.

[16] N. Chittock, M. Vos, T. Faraz, W. Kessels, H. Knoops, A. Mackus, Isotropic plasma atomic layer etching of Al2O3 using a fluorine containing plasma and Al(CH3)3, Appl. Phys. Lett. 117 (16) (2020), 162107, https://doi.org/10.1063/5.0022531.

[17] N. Johnson, H. Sun, K. Sharma, S. George, Thermal atomic layer etching of crystalline aluminum nitride using sequential, self-limiting hydrogen fluoride and

Sn(acac)2 reactions and enhancement by H2 and Ar plasmas, J. Vac. Sci. Technol. 34 (5) (2016), 050603, https://doi.org/10.1116/1.4959779.
[18] Y. Lee, Z. Zhou, D. Danner, P. Fryer, J. Harper, Chemical sputtering of Al2O3 by fluorine-containing plasmas excited by electron cyclotron resonance, J. Appl. Phys. 68 (10) (1990) 5329–5336, https://doi.org/10.1063/1.347027.
[19] X. Li, X. Hua, L. Ling, G. Oehrlein, M. Barela, H. Anderson, Fluorocarbon-based plasma etching of SiO2: comparison of C4F6/Ar and C4F8/Ar discharges, J. Vac. Sci. Technol.: Vacu, Surf. Films. 20 (6) (2002) 2052, https://doi.org/10.1116/1.1517256.
[20] T. Standaert, C. Hedlund, E. Joseph, G. Oehrlein, T. Dalton, Role of fluorocarbon film formation in the etching of silicon, silicon dioxide, silicon nitride, and amorphous hydrogenated silicon carbide, J. Vac. Sci. Technol.: Vacu, Surf. Films. 22 (1) (2004) 53–60, https://doi.org/10.1116/1.1626642.
[21] D. Marra, E. Aydil, Effect of H2 addition on surface reactions during CF4/H2 plasma etching of silicon and silicon dioxide films, J. Vac. Sci. Technol.: Vacu, Surf. Films. 15 (5) (1997) 2508–2517, https://doi.org/10.1116/1.580762.
[22] J. Lee, A. Efremov, K.-H. Kwon, On the relationships between plasma chemistry, etching kinetics and etching residues in CF4+C4F8+Ar and CF4+CH2F2+Ar plasmas with various CF4/C4F8 and CF4/CH2F2 mixing ratios, Vacuum 148 (2018) 214–223, https://doi.org/10.1016/j.vacuum.2017.11.029.
[23] C. Lee, K. Kanarik, R. Gottscho, The grand challenges of plasma etching: a manufacturing perspective, J. Phys. D Appl. Phys. 47 (27) (2014), 273001, https://doi.org/10.1088/0022-3727/47/27/273001.
[24] T. Faraz, Y.G.P. Verstappen, M.A. Verheijen, N.J. Chittock, J.E. Lopez, E. Heijdra, W.J.H. van Gennip, W.M.M. Kessels, A.J.M. Mackus, Precise ion energy control with tailored waveform biasing for atomic scale processing, J. Appl. Phys. 128 (2020), 213301, https://doi.org/10.1063/5.0028033.
[25] A.V. Miakonkikh, A.V. Shishlyannikov, A.A. Tatarintsev, V.O. Kuzmenko, K. V. Rudenko, E.S. Gornev, Study of the plasma resistance of a high resolution e-beam resist HSQ for prototyping nanoelectronic devices, Russ. Microelectron. 50 (5) (2021) 297–302, https://doi.org/10.1134/S1063739721050048.
[26] G. Greczynski, L. Hultman, X-ray photoelectron spectroscopy: towards reliable binding energy referencing, Prog. Mater. Sci. 107 (2020), 100591, https://doi.org/10.1016/j.pmatsci.2019.100591.
[27] J.A. Taylor, G.M. Lancaster, J.W. Rabalais, Surface alteration of graphite, graphite monofluoride and teflon by interaction with Ar+ and Xe+ beams, Appl. Surf. Sci. 1 (1978) 503–514, https://doi.org/10.1016/0378-5963(78)90027-2.
[28] J.J. Pireaux, J.P. Delrue, A. Hecq, J.P. Dauchet, in: K.L. Mittal (Ed.), Physico-Chemical Aspects of Polymer Surfaces, vol. 1, Plenum, New York, 1983, pp. 53–81.
[29] D.F. O'kane, D.W. Rice, Preparation and characterization of glow discharge fluorocarbon-type polymers, J. Macromol. Sci. Part A - Chemistry: Pure and Applied Chemistry 10 (1976) 567–577, https://doi.org/10.1080/00222337608061200.
[30] K.V. Rudenko, A.V. Myakon'kikh, A.A. Orlikovsky, A.N. Pustovit, New method for the Langmuir probe diagnostics of polymerizing plasmas, Russ. Microelectron. 36 (1) (2007) 14–26, https://doi.org/10.1134/S1063739707010027.
[31] F. Chen, Langmuir probes in RF plasma: surprising validity of OML theory, Plasma Sources Sci. Technol. 18 (3) (2009), 035012, https://doi.org/10.1088/0963-0252/18/3/035012.
[32] D. Lopaev, A. Volynets, S. Zyryanov, A. Zotovich, A. Rakhimov, Actinometry of O, N and F atoms, J. Phys. D Appl. Phys. 50 (7) (2017), 075202, https://doi.org/10.1088/1361-6463/50/7/075202.
[33] L.D.B. Kiss, J.-P. Nicolai, W.T. Conner, H.H. Sawin, CF and CF2 actinometry in a CF4/Ar plasma, J. Appl. Phys. 71 (1992) 3186, https://doi.org/10.1063/1.350961.
[34] A. Zotovich, O. Proshina, Z. el Otell, D. Lopaev, T. Rakhimova, A. Rakhimov, et al., Comparison of vacuum ultra-violet emission of Ar/CF4and Ar/CF3I capacitively coupled plasmas, Plasma Sources Sci. Technol. 25 (5) (2016), 055001, https://doi.org/10.1088/0963-0252/25/5/055001.
[35] I. Chun, A. Efremov, G.Y. Yeom, K.-H. Kwon, A comparative study of CF4/O2/Ar and C4F8/O2/Ar plasmas for dry etching applications, Thin Solid Films 579 (2015) 136, https://doi.org/10.1016/j.tsf.2015.02.060.
[36] R. d'Agostino, F. Cramarossa, S. De Benedictis, Diagnostics and decomposition mechanism in radio-frequency discharges of fluorocarbons utilized for plasma etching or polymerization, Plasma Chem. Plasma Process. 2 (3) (1982) 213–231.
[37] Rozum, I., Limão-Vieira, P., Eden, S., Tennyson, J., & Mason, N. J. (2006). Electron Interaction Cross Sections for and Radicals. J. Phys. Chem. Ref. Data, 35, 267. https://doi.org/10.1063/1.2149379.
[38] https://srdata.nist.gov/xps/elm_Spectra_query.aspx?Elm1=F&LD1=1s&Elm2=&LD2=&Elm3=&LD3=&Elm4=&LD4=&sType=PE, last accessed 30/09/2022, https://doi.org/10.18434/T4T88K.
[39] M. Schaepkens, T.E.F.M. Standaert, N.R. Rueger, P.G.M. Sebel, G.S. Oehrlein, J. M. Cook, Study of the SiO 2 -to- Si 3 N 4 etch selectivity mechanism in inductively coupled fluorocarbon plasmas and a comparison with the SiO 2 -to-Si mechanism, J. Vac. Sci. Technol. 17 (1) (1999) 26–37, https://doi.org/10.1116/1.582108.
[40] X. Wang, X. Xu, Y. Liu, Y. Hong, S. Fu, Reactive ion beam etching of HfO2 film using Ar/CHF3 gas chemistries, in: Proc. SPIE 5636, Holography, Diffractive Optics, and Applications II, 2005, p. 576, https://doi.org/10.1117/12.573666.
[41] N. Louvain, Z. Karkar, M. El-Ghozzi, P. Bonnet, K.P. Guérin, P. Willmann, Fluorination of anatase TiO2 towards titanium oxyfluoride TiOF2: novel synthesis approach and proof of Li-insertion mechanism, J. Mater. Chem. 2 (2014) 15308–15315, https://doi.org/10.1039/C4TA02553A.
[42] https://webbook.nist.gov/cgi/inchi?ID=C7783611&Mask=4. (Accessed 30 September 2022).
[43] T. Song, M. Yang, J. Chai, M. Callsen, J. Zhou, T. Yang, et al., The stability of aluminium oxide monolayer and its interface with two-dimensional materials, Sci. Rep. 6 (1) (2016), https://doi.org/10.1038/srep29221.